AIAA-2000-1949

# Evaluation of an Impedance Model for Perforates Including the Effect of Bias Flow

J. F. Betts
Virginia Tech
Virginia Consortium of Engineering and Science Universities
Hampton, VA 23666

J. I. Follet
University of Virginia
Virginia Consortium of Engineering and Science Universities
Hampton, VA 23666

J. J. Kelly
Virginia Tech
Virginia Consortium of Engineering and Science Universities
Hampton, VA 23666

and

R. H. Thomas
NASA Langley Research Center
Hampton, VA 23681

**6th AIAA/CEAS**
**Aeroacoustics Conference**
12-14 June 2000 / Lahaina, Hawaii

# EVALUATION OF AN IMPEDANCE MODEL FOR PERFORATES INCLUDING THE EFFECT OF BIAS FLOW

Juan F. Betts*, Jesse I. Follet†, Jeffrey J. Kelly‡
Virginia Polytechnic Institute and State University
Virginia Consortium of Engineering and Science Universities
303 Butler Farm Road, Suite 101
Hampton, VA 23666

and

Russell H. Thomas§
NASA Langley Research Center
Hampton, VA 23681

A new bias flow impedance model is developed for perforated plates from basic principles using as little empiricisms as possible. A quality experimental database was used to determine the predictive validity of the model. Results show that the model performs better for higher (15%) rather than lower (5%) percent open area (POA) samples. Based on the least squares ratio of numerical vs. experimental results, model predictions were on average within 20% and 30% for the higher and lower (POA), respectively. It is hypothesized on the work of other investigators that at lower POAs the higher fluid velocities in the perforate's orifices start forming unsteady vortices, which is not accounted for in our model. The numerical model, in general also underpredicts the experiments. It is theorized that the actual acoustic $C_D$ is lower than the measured raylometer $C_D$ used in the model. Using a larger $C_D$ makes the numerical model predict lower impedances. The frequency domain model derived in this paper shows very good agreement with another model derived using a time domain approach.

## Nomenclature

| | |
|---|---|
| c | speed of sound in the normal incidence tube |
| $C_D$ | discharge coefficient |
| d | perforate hole diameter |
| f | frequency |
| $J_0$ | Bessel function of zeroth order |
| $J_1$ | Bessel function of first order |
| $J_2$ | Bessel function of second order |
| k | $2\pi f/c$ |
| L | length of cavity |
| M | Mach number in the cavity |
| $M_H$ | effective Mach number in the holes of the perforate plates |
| p | pressure in the fluid |
| $p_a$ | acoustic pressure in cavity |
| $p_{ah}$ | acoustic pressure in perforate's orifice |
| t | perforate thickness |
| T | period |
| $\tilde{v}$ | fluid particle velocity |
| $v_a$ | acoustic particle velocity in the normal incidence tube |
| $v_{ah}$ | acoustic particle velocity in perforate's orifice |
| $v_b$ | bias flow velocity in the cavity |
| $v_{bh}$ | bias flow velocity in the perforate's orifice |
| $v_{rms}$ | rms acoustic particle velocity |
| $\chi$ | normalized reactance |
| $\mu$ | absolute viscosity of fluid |
| $\mu'$ | effective viscosity |

---

* Graduate Research Assistant, Mechanical Engineering Department, Member AIAA.
† Graduate Research Assistant, Department of Mechanical, Aerospace, and Nuclear Engineering University of Virginia, Member AIAA.
‡ Research Associate Professor, Mechanical Engineering Department, Senior Member AIAA.
§ Aerospace Engineer, Aeroacoustics Branch, Senior Member AIAA.

| | |
|---|---|
| $\theta$ | normalized resistance |
| $\rho$ | density of fluid (air) |
| $\sigma$ | percent open area |
| $\tau$ | time |
| $\omega$ | $2\pi f$ |
| $\xi$ | normalized impedance |

Throughout this paper acoustic impedance is normalized with respect to $\rho c$. The convection $\xi = -p_a/\rho c v_a$ and $e^{+i\omega\tau}$ is used unless otherwise indicated.

## Introduction

Due to the current and projected concerns about community noise annoyance from commercial air traffic, a number of enhanced abatement designs are being considered. One concept for improving suppression efficiency is the bias flow liner. Bias flow has been previously investigated by Dean, who conducted an initial proof-of-concept study that showed several potential advantages[1]. In-situ control of liner impedance would allow several desirable possibilities including optimizing liner impedance to match different operating conditions or to more accurately match design conditions that could not be reached due to manufacturing tolerances.

The purpose of this study is to develop a bias flow impedance model from basic principles with as little empiricisms as possible and validate this model using quality experiments produced for this purpose from the NASA Langley Normal Incidence Tube (NIT). The experimental database included both fibermetal and perforate samples that were tested with and without bias flow in a single-degree-of-freedom liner configuration.[2]

A validation error criterion was developed and used as a standard for determining the validity of the numerical model results.

## Previous Bias Flow Corrections

Dean developed a bias flow model in his initial proof-of-concept study (Ref. 1) of bias flow effect on liner impedance. His model is based on principles outlined by Hersh and Rogers.[3] Dean essentially replaced the acoustic particle velocity with the bias flow velocity in the Hersh and Rogers' model without further justification except to say that the bias flow velocity was much greater than the acoustic particle velocity. As will be shown later, replacing the acoustic velocity with the bias flow velocity is questionable.

In the NASA Langley Zwikker-Kosten Transmission Line Code (ZKTL)[4], bias flow is accounted for by replacing the acoustic particle velocity in the impedance models with

$$v_a + v_b \tag{1}$$

This correction seems more reasonable than Dean's correction, especially at low bias flow velocities. Nevertheless, this bias flow correction as well as Dean's correction does not follow from basic principles.

In another study, Premo derived a bias flow model using a time-domain approach. This approach yielded the following replacement for the acoustic particle velocity to include bias flow[5]

$$\sqrt{(1.15v_{rms})^2 + (2v_b)^2} \tag{2}$$

## Development of A New Bias Flow Model

The linear part of the following derivation follows from the principles outlined by Crandall of the impedance of a single tube.[6] The momentum equation for a viscous fluid is

$$\rho\left[\frac{\partial \bar{v}}{\partial \tau} + (\bar{v}\bullet\nabla)\bar{v}\right] = -\nabla p + \mu\nabla^2\bar{v} \tag{3}$$

where the compressibility term $\frac{1}{3}\mu\nabla(\nabla\bullet\bar{v})$ is assumed small and therefore is omitted from Eq. (3). Note, that by making this approximation density disturbances are ignored. Let any fluid variable q be the sum of a mean flow $q_b$ and an acoustic component $q_a$, that is

$$q = q_b + q_a \tag{4}$$

Substituting Eq. (4) into Eq. (3) and expanding yields

$$\begin{aligned}\rho\Big[&\frac{\partial \bar{v}_a}{\partial \tau} + (\bar{v}_b\bullet\nabla)\bar{v}_b + (\bar{v}_b\bullet\nabla)\bar{v}_a \\ &+ (\bar{v}_a\bullet\nabla)\bar{v}_b + (\bar{v}_a\bullet\nabla)\bar{v}_a\Big] \\ &= -\nabla p_b - \nabla p_a + \mu\nabla^2\bar{v}_b + \mu\nabla^2\bar{v}_a\end{aligned} \tag{5}$$

This equation contains bias flow only, coupled bias flow/acoustic, and acoustic only components. The bias flow only components should balance, leaving coupled and acoustic only components. Furthermore, assume that perforate holes can be modeled as cylindrical ducts, and that the velocity has components in the x and r direction along the length and radius of the perforate hole respectively. So far, the above description pertains

to the interior of the perforate hole. To indicate this, the variables $v_a$ and $v_b$ will be subscripted with $v_{ah}$ and $v_{bh}$. Making these approximations to Eq. (5) produces

$$\rho\left[\frac{\partial v_{ah}}{\partial \tau}+v_{bh}\frac{\partial v_{ah}}{\partial x}+v_{ah}\frac{\partial v_{bh}}{\partial x}+v_{ah}\frac{\partial v_{ah}}{\partial x}\right] = -\frac{\partial p_{ah}}{\partial x}+\mu\left(\frac{\partial^2 v_{ah}}{\partial r^2}+\frac{1}{r}\frac{\partial v_{ah}}{\partial r}+\frac{\partial^2 v_{ah}}{\partial x^2}\right) \tag{6}$$

Rewriting Eq. (6) and grouping linear and nonlinear coupling terms yields

$$\rho\frac{\partial v_{ah}}{\partial \tau}-\mu\left(\frac{\partial^2 v_{ah}}{\partial r^2}+\frac{1}{r}\frac{\partial v_{ah}}{\partial r}+\frac{\partial^2 v_{ah}}{\partial x^2}\right) +\rho\left(v_{bh}\frac{\partial v_{ah}}{\partial x}+v_{ah}\frac{\partial v_{bh}}{\partial x}+v_{ah}\frac{\partial v_{ah}}{\partial x}\right) = -\frac{\partial p_{ah}}{\partial x} \tag{7}$$

The right hand side of Eq. (7) can be written as

$$-\frac{\partial p_{ah}}{\partial x}=-\left(\left.\frac{\partial p_{ah}}{\partial x}\right|_{linear}+\left.\frac{\partial p_{ah}}{\partial x}\right|_{nonlinear}\right) \tag{8}$$

Therefore the linear and nonlinear terms of Eq. (8) balance their corresponding counterparts respectively, in Eq. (7). By utilizing the definition of normalized impedance, the linear term of Eq. (8) can be rewritten in terms of the linear non-dimensional impedance by noting that

$$\left.-\frac{\partial p_{ah}}{\partial x}\right|_{linear}=\xi_{linear}\rho c\frac{\partial v_{ah}}{\partial x} \tag{9}$$

Substituting the above relationship into Eq. (7) and assuming $\partial x=t$, $p_{ah}=p_a$, $\partial p_a=p_a$, and $\partial v_a=v_a$ produces

$$-\xi_{linear}\rho c v_{ah}-\rho\left(v_{bh}v_{ah}\right)-\frac{\rho v_{ah}^2}{2}=p_a \tag{10}$$

From continuity, the relationship between the incident and hole velocities for an incompressible fluid is given by

$$v_a=C_D\sigma v_{ah} \qquad v_b=C_D\sigma v_{bh} \tag{11}$$

Inserting the relationships in Eq. (11) into Eq. (10) and multiplying by $v_a$ produces

$$-\frac{\xi_{linear}\rho c v_a^2}{C_D\sigma}-\frac{\rho}{(C_D\sigma)^2}v_b v_a^2-\frac{\rho v_a^3}{2(C_D\sigma)^2}=p_a v_a \tag{12}$$

Integrating both sides of Eq. (12) over a period yields

$$-\frac{1}{T}\int_0^T\frac{\xi_{linear}\rho c v_a^2}{C_D\sigma}d\tau-\frac{1}{T}\int_0^T\frac{\rho}{(C_D\sigma)^2}v_b v_a^2 d\tau -\frac{1}{T}\int_0^T\frac{\rho|v_a|v_a^2}{2(C_D\sigma)^2}d\tau=-\frac{1}{T}\int_0^T\xi\rho c v_a^2 d\tau \tag{13}$$

where $v_a$ and $p_a$ is assumed to be a harmonic solution with respect to time $\cos(\omega\tau)$. In Eq. (13) $v_a^3$ is replaced by $|v_a|v_a^2$ so that this term remains positive. Simplifying this equation results in

$$\frac{\xi_{linear}\rho c}{C_D\sigma}v_{rms}^2+\frac{\rho}{(C_D\sigma)^2}v_b v_{rms}^2 +\frac{\rho}{2(C_D\sigma)^2}\frac{4}{3\pi}2.828v_{rms}^3=\xi\rho c v_{rms}^2 \tag{14}$$

Dividing both sides by $\rho c v_{rms}^2$ produces

$$\xi=\frac{\xi_{linear}}{C_D\sigma}+\frac{1}{2c(C_D\sigma)^2}\left[2v_b+1.2v_{rms}\right] \tag{15}$$

Melling notes that the pressure drop across a "sharp edge" orifice has been studied in some detail[7]. From these studies, a departure from the nonlinear term in Eq. (15) is suggested. Making the corrections indicated by Melling to Eq. (15) yields

$$\xi=\frac{\xi_{linear}}{C_D\sigma}+\frac{1-\sigma^2}{2c(C_D\sigma)^2}\left[2v_b+1.2v_{rms}\right] \tag{16}$$

The linear impedance ($\xi_{linear}$) term is determined by solving Eq. (7) utilizing only the linear terms. Writing that equation leaving only the linear term yields

$$\rho\frac{\partial v_{ah}}{\partial \tau}-\mu\left(\frac{\partial^2 v_{ah}}{\partial r^2}+\frac{1}{r}\frac{\partial v_{ah}}{\partial r}+\frac{\partial^2 v_{ah}}{\partial x^2}\right) =-\left.\frac{\partial p_{ah}}{\partial x}\right|_{linear} \tag{17}$$

Melling summarizes Crandal's solution to Eq. (17) assuming that the term $\partial^2 v_{ah}/\partial x^2 \to 0$, which effectively eliminates any acoustic waves traveling

along the length of the duct. The impedance solution to Eq.(17) is

$$\xi = \frac{1}{c}\frac{i2\pi ft}{F\left[\frac{k_s d}{2}\right]} \tag{18}$$

where

$$F\left(\frac{k_s d}{2}\right) = 1 - \frac{2J_1\left(\frac{k_s d}{2}\right)}{k_s \frac{d}{2} J_0\left(\frac{k_s d}{2}\right)} \tag{19}$$

Sivian showed that the viscosity inside the perforate hole along a highly thermally conductive wall was different from the absolute viscosity outside the hole[8]. It was shown in this study that for air over a wide range of temperatures, the relationship between $\mu$ and $\mu'$ is

$$\mu' = 2.179\mu \tag{20}$$

Noting that the analysis for the impedance was done within the perforate's hole $k_s$ becomes $k_s'$. Tijdeman has studied extensively the propagation of sound waves in cylindrical tubes[9]. He presents results of acoustic propagation in ducts under less restrictive assumptions, than what has been presented here. His results could be used as a starting point in developing a more comprehensive impedance model.

Melling also describes contributions by Sivian and Ingard for end effects to the perforate hole, and Fok's contribution to interaction effects between holes. This analysis is not going to be repeated here, but the results will be included. Therefore the Perforate Bias Flow (PBF) model is

$$\xi = \frac{1}{c\sigma C_D}\left[\frac{i2\pi ft}{F\left[\frac{k_s' d}{2}\right]} + \frac{8d}{3\pi F\left[\frac{k_s d}{2}\right]\psi'(\sigma)}\right] + \frac{(1-\sigma^2)}{2c(\sigma C_D)^2}\left[2v_b + 1.2v_{rms}\right] \tag{21}$$

and the Fok function $\psi'(\sigma)$ is defined as[10]

$$\psi'(\sigma) = \sum_{n=0}^{8} a_n \left(\sqrt{\sigma}\right)^n \tag{22}$$

where

$a_0$=1.0 $a_1$=-1.4092 $a_2$=0.0
$a_3$=0.33818 $a_4$=0.0 $a_5$=0.06793
$a_6$=-0.02287 $a_7$=0.003015 $a_8$=-0.01614

Note that the PBF model implies a bias flow correction to existing impedance models, where the acoustic particle velocity is replaced by

$$2v_b + 1.2v_{rms} \tag{23}$$

A problem arises when large enough negative bias flow rates would lead to negative impedance values. A recent study has experimentally shown the effect of negative bias flow rates of two degree-of-freedom liners.[11] The results of this suggest that increasing negative bias flow rates do not necessarily lead to lower or negative impedances. Consequently, Eq. (23) needs to be restricted to positive values. A possible method to accomplish this is to square Eq. (23) and take its square root. Doing this produces

$$v_a = \sqrt{1.44v_{rms}^2 + 4v_b^2 + 4.8v_{rms}v_b} \tag{24}$$

Thus the sign of $v_b$ does affect the magnitude of impedance but cannot drive it negative. Therefore, blowing produces a different impedance result than suction.

Eq. (21) has a low and high frequency approximation. These approximations are valid if

$$\frac{d}{2}\sqrt{\frac{2\pi f\rho}{\mu}} < 1 \qquad \frac{d}{2}\sqrt{\frac{2\pi f\rho}{\mu}} > 10 \tag{25}$$

respectively. The low and high frequency approximations of Eq. (21) are

$$\xi = \frac{32\mu t}{\rho c\sigma C_D d^2} + \frac{(1-\sigma^2)}{2c(\sigma C_D)^2}\left[2v_b + 1.2v_{rms}\right] + i\frac{2\pi f}{\sigma c C_D}\left(\frac{4}{3}t + \frac{8d}{3\pi\psi'(\sigma)}\right) \tag{26}$$

$$\xi = 2.82\frac{\sqrt{2\pi\left(\mu/\rho\right)f}}{c\sigma C_d}\frac{t}{d} + \frac{(1-\sigma^2)}{2c(\sigma C_D)^2}\left[2v_b + 1.2v_{rms}\right] + i\left(\frac{2\pi ft}{c\sigma C_D} + 2.82\frac{\sqrt{2\pi\left(\mu/\rho\right)f}}{c\sigma C_d}\frac{t}{d} + \frac{8}{3\pi}\frac{d}{\psi'(\sigma)}\right) \tag{27}$$

respectively. The PBF model runs into the problem that the Bessel functions in the linear component of the impedance obscure its physical relationship to geometrical parameters such as $\sigma$, t, and d. The

low and high frequency approximations to the PBF model do not account for intermediate frequencies. Therefore, a single model that does not contain the Bessel functions, and "works" for all frequencies is desirable. One such correction similar to one done by Kraft, Yu, and Kwan, is[12]

$$\xi = \frac{16\mu t}{\rho c \sigma C_D d^2} + 2.82\frac{\sqrt{2\pi\left(\mu/\rho\right) f}}{c\sigma C_d}\frac{t}{d} + \frac{(1-\sigma^2)}{2c(\sigma C_D)^2}[2v_b + 1.2v_{rms}] + i\left(\frac{2\pi f t}{c\sigma C_D} + 2.82\frac{\sqrt{2\pi\left(\mu/\rho\right) f}}{c\sigma C_d}\frac{t}{d} + \frac{8}{3\pi}\frac{d}{\psi'(\sigma)}\right) \quad (28)$$

Equation (28) will be called the Perforate Bias Flow Intermediate Frequency model or PBFIF model.

Effective Mach Number

$M_H$ is the effective Mach number at the perforate hole. It is defined as

$$M_H = \frac{v_{ah} + 2v_{bh}}{2c} \quad (29)$$

The problem with using this equation is that the actual $v_{ah}$ is unknown as far as the impedance models are concerned. In fact that is what the impedance models are trying to find. The experimental $v_{ah}$ could be acquired from the experimental results and an assumed relationship between the incident and perforate hole acoustic particle velocities. Although this method would be the most accurate, a simplified approach suffices for this study.

It is of interest to find out at what level of bias flow, do changes in $M_H$ due to SPL changes, not affect the overall acoustic impedance. Consequently, for a plane wave, the relationship between the acoustic particle velocity and pressure can be used to determine an approximate magnitude of $v_{ah}$. Therefore, the relationship between the acoustic particle velocity and the SPL is

$$|v_{ah}| = \frac{P_{ref} 10^{SPL/20}\sqrt{2}}{\rho c} \quad (30)$$

Using the continuity principle for an incompressible fluid to relate the incident velocity and the hole velocity and Eqs. (29) and (30) yields

$$|M_H| = \frac{1}{2c\sigma C_D}\left[\frac{P_{ref} 10^{SPL/20}\sqrt{2}}{\rho c} + 2v_b\right] \quad (31)$$

where $|M_H|$ is used to indicate the magnitude of the Mach number in the perforate.

Validation Error Criteria

The method of least squares can be employed to establish the validation criteria for the model predictions. Let $E_i$ and $N_i$ be a set of experimental and numerical results, respectively. Assume that the following relationship exists between $E_i$ and $N_i$[13]

$$N_i = SE_i + e_i \quad (32)$$

where $e_i$ is the random error associated with experiment i and S is an arbitrary constant. Minimizing the square of the errors yields the linear regression of $N_{estimate}$ on E where

$$S = \frac{\sum_{i=1}^{m} N_i E_i}{\sum_{i=1}^{m} E_i^2} \quad (33)$$

thus $N_{estimate}=SE_i$ Note that this regression curve has been forced thru zero. S measures the ratio of numerical results to experimental results. If the ratio is equal to one then the experimental values equal the numerical results. Therefore, the deviation of this ratio from one is indicative of the least squares bias of the numerical vs. experimental results.

The correlation coefficient is indicative of the random error in the predictions and is given by[14]

$$C = \frac{\sum_{i=1}^{m}(E_i - \bar{E})(N_i - \bar{N})}{\sqrt{\sum_{i=1}^{m}(E_i - \bar{E})^2 \sum_{i=1}^{m}(N_i - \bar{N})^2}} \quad (34)$$

where, as before, E and N stand for experimental and numerical results, respectively. The correlation coefficient goes form –1 to +1 if the data is negatively or positively correlated, respectively. Note that in this case the regression

curve has not been constrained to pass thru N=E=0.

## Model Validation

Figure 1 shows the experimental vs. the PBFIF model impedance results for a representative sample with no flow. The numerical results approach the experimental results as the sound pressure level is increased in both the resistance and reactance. The slope and correlation error criteria for both the resistance and reactance show continuous improvements as the sound pressure level is increased (See Table 1). This indicates that the nonlinear term in the PBFIF model, which is associated with the acoustic particle velocity better models the experiments, than the linear component of this model.

Figure 2 shows the experimental and PBFIF model impedance at 130 dB and 5 % nominal (5.92 % actual) POA for various bias flow velocities. The figure shows increasing resistance with increasing bias flow rates. The resistance seems to stay constant with frequency except for the high bias flow rates, where it tends to decrease with increasing frequency. The reactance increases with frequency due to the cavity reactance. The experimental reactance tends to decrease as bias flow is increased. The model was not able to account for this effect.

Figure 3 shows the slope and correlation error criteria for the resistance for various t/d samples. The flow rates are given in cm/s and $M_H$ (Hole Mach Number) for the NIT and hole velocities, respectively on the x-axis. The slope error criteria shows a mean slope starting at one for no flow then decreasing to 0.7 and increasing back to 0.9 as flow rate is increased. Therefore, the resistance numerical and experimental results are staying within 30% of each other in a least squares sense.

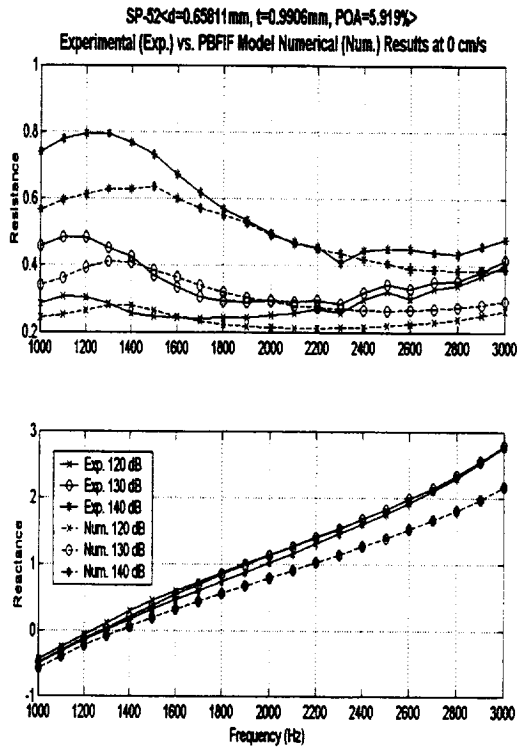


**Figure 1.** Experimental impedance vs. PBFIF model numerical predictions for a sample with POA=5.92.

**Table 1.** Slope and Correlation Coefficients results in Fig. 1.

| | Slope | Correlation |
|---|---|---|
| Resistance | | |
| 120 dB | 0.8127 | 0.2509 |
| 130 dB | 0.8692 | 0.6413 |
| 140 dB | 0.8670 | 0.9290 |
| Reactance | | |
| 120 dB | 0.7552 | ≈1.000 |
| 130 dB | 0.7604 | ≈1.000 |
| 140 dB | 0.7865 | ≈1.000 |

The model underpredicts the resistances for all bias flow rates. At the higher flow rates the slope error improves because the experimental resistance decreases with increasing frequency at these flow rates (See Fig. 2). Since the model underpredicts the resistance, the decrease with frequency places the experimental resistance closer to the model results, and therefore decreases the measured slope error.

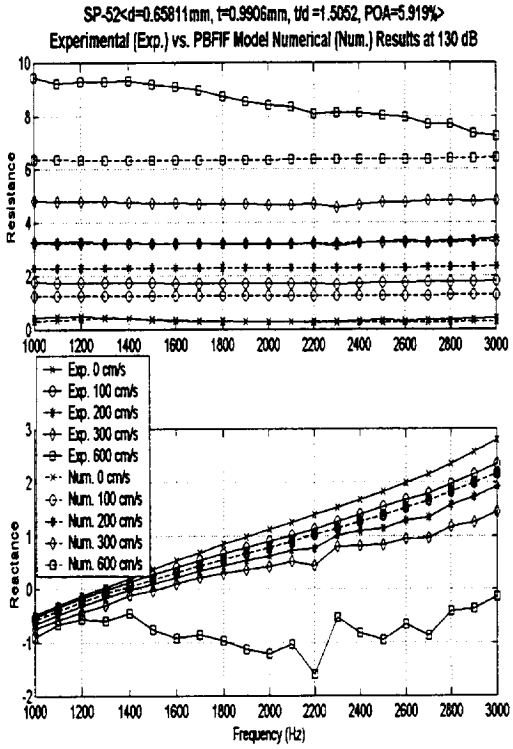


**Figure 2.** Experimental impedance vs. PBFIF model numerical predictions for a sample with POA=5.92.

The mean correlation increases from 0.45 to 0.65 and then goes negative. Part of the reason for the low correlation numbers is the low variability with frequency that these impedance curves have (See Fig. 2). Since the correlation measures the percentage change in experiments accounted by the model, low variation increases the errors.

Figure 4 shows the slope and correlation error criteria for the reactance of the same t/d samples. The mean reactance slope starts at 0.7 goes to 1.1 and then decreases to negative values as bias flow is increased. The mean correlation on the other hand stays close to one at the lower bias flow rates and then sharply decreases to 0.65.

Note that there is significant scatter in Fig. 3 and 4 for the various t/d samples. This scatter is low at no flow, but significant for nearly all the flow rates. This result indicates that there is some sort of interaction between t/d and bias flow velocities not accounted for by the PBFIF model.

Jing and Sun[15,16] provide possible explanations for the scatter in error associated with various t/d, and the impedance values at higher bias flow rates. They developed two models, one that looked into the nonlinear properties of the hole and another that accounted for bias flow.

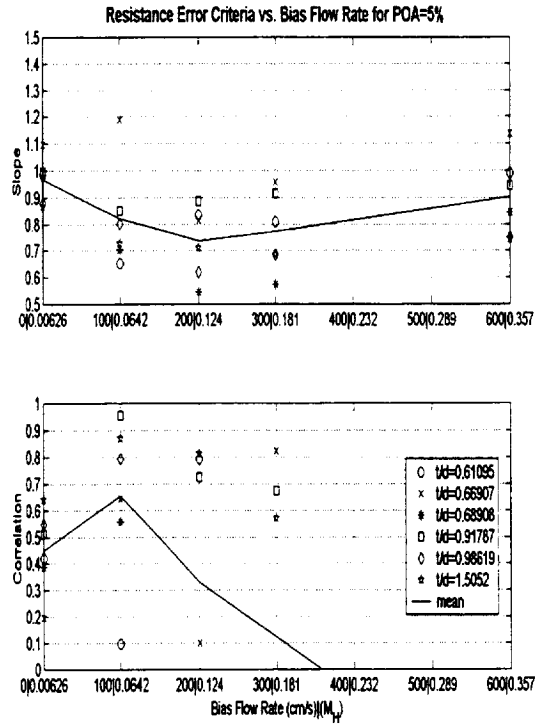


**Figure 3.** PBFIF model resistance error criteria for POA=5.

Jing and Sun (Ref. 18) took issue with the empirical nature of the determination of $C_D$. Their model showed that the formation of the vena contracta is a time dependent problem in the presence of an acoustic field, and determined an approximate steady state value of 0.61 for $C_D$. This value of $C_D$ is lower than the normally measured experimental value of 0.76 or higher. This possibly explains why the PBFIF model underpredicts the resistance experiments since a higher $C_D$ produces lower predicted resistance results.

Jing and Sun (Ref. 19) developed a boundary element bias flow model from Euler's Equation, where the Kutta condition was applied to generate unsteady vortices due to the bias flow. Their model showed that different t/d and hole Mach numbers had a significant impact in the resistance and reactance. Their model successfully predicted a decrease in reactance as bias flow was increased. Since the PBFIF model does not take into account vortex creation in the perforate's holes, it fails to predict the decrease in reactance, as well as, some of the interaction between hole Mach number and changes in t/d. This possibly explains the scatter seen in the error

plots with t/d, which suggest that the models are not accounting for some physical phenomena associated with t/d.

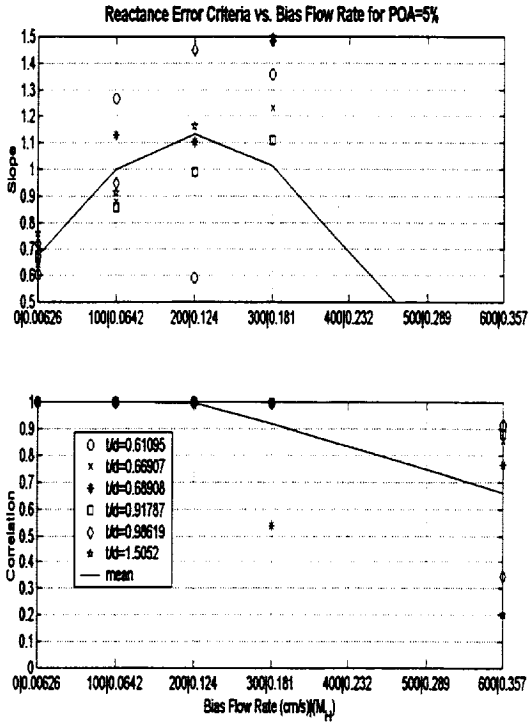


**Figure 4.** PBFIF model reactance error criteria for POA=5.

The PBFIF model improves its prediction as POA is increased. Figure 5 shows the experimental and PBFIF model impedance at 130 dB and 15% nominal (16.48% actual) POA for various bias flow velocities. The figure shows the experimental and numerical results are closer at 15% than at 5 % (Fig. 2) POA. The mean slope and correlation error criteria for both the resistance and reactance show significant improvements as seen in Figs. 6 and 7. The error plots also show significant reduction in scatter due to different t/d, indicating that the PBFIF model can better account for changes in t/d at this higher POA.

For the resistance, the mean slope criteria goes from about 0.9 at zero flow to 1.2 and down to .8 in Fig. 6, indicating that the numerical and experimental results stay on average within 20% of each other. The correlation shows improvement, but still exhibits poor correlation in part due to the low variability in resistance curves. The reactance slope criteria starts around 0.8 and steadily increases to one, indicating that the reactance curves are within 20% of the experiments. The reactance correlation is about one for all flow rates indicating a nearly perfect correlation between the experimental and numerical results.

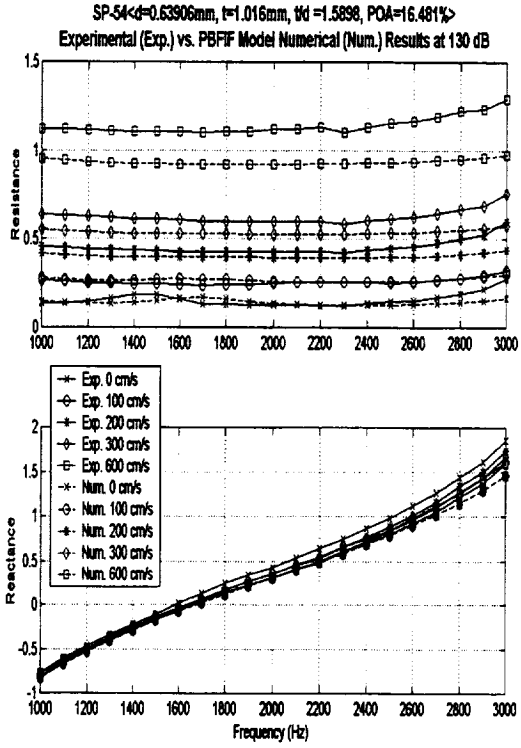


**Figure 5.** Experimental impedance vs. PBFIF model numerical predictions for a sample with POA=16.48.

There is a possible explanation for the PBFIF model's improved performance as POA is increased. As POA is increased, the effective bias flow Mach number in the perforate hole decreases. For example, the highest Mach number achieved with the 15% and 5% POA samples was 0.126 (See Figs. 6 and 7) and 0.357 (See Figs. 3 and 4), respectively. The PBFIF model performs better at lower flow velocities, because the formation of unsteady vortices is a function of the fluid velocity, given constant viscosity and hole diameter. At low flow velocities vortices are not formed, and the perforate's hole physics follow the principles outlined in the PBFIF model. As the bias flow velocity in the hole increases, unsteady vortices start forming and the assumptions and principles outlined in the PBFIF model start to break down. At higher perforate bias flow rates a model such as that outlined in Ref. 19 should be used.

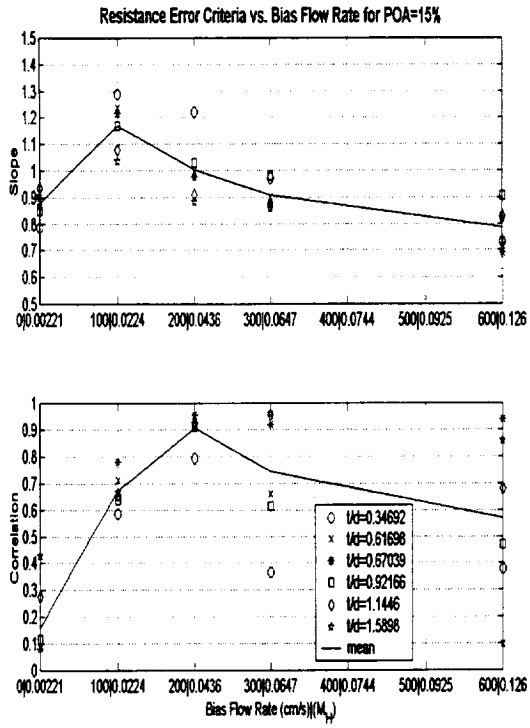


**Figure 6.** PBFIF model resistance error criteria for POA=15.

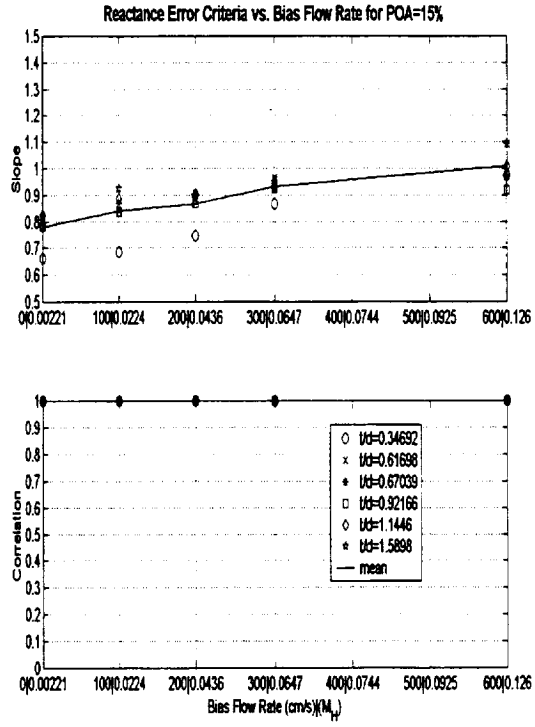


**Figure 7.** PBFIF model reactance error criteria for POA=15.

The PBFIF model implies a bias flow correction given by Eq. (23) as indicated earlier. This correction, which was derived using a frequency domain approach, is similar to that developed by Premo (Ref. 6) using a time domain approach (See Eq. (2)). Figures 8 and 9 show resistance comparisons between the models for a 5% and 15% POA sample perforates. The reactance is not shown because bias flow only affects the resistance in both Premo's and the PBFIF model. These figures show almost identical resistance values for all bias flow rates.

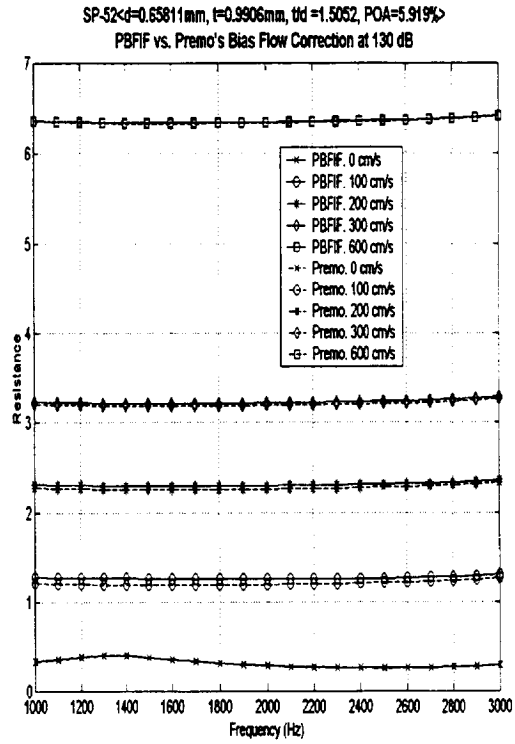


**Figure 8.** PBFIF vs. Premo's impedance model predictions at POA=5.92.

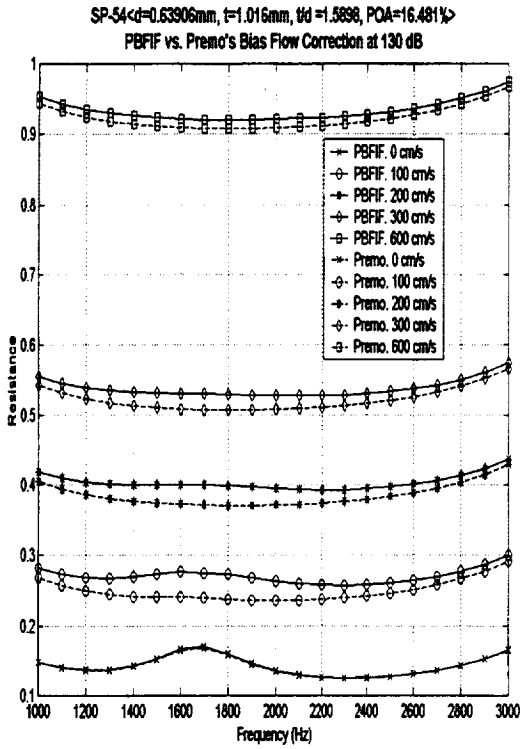


**Figure 9.** PBFIF vs. Premo's impedance model predictions at POA=16.48.

## Conclusions

The numerical results in general underpredict the experiments. The validation error criteria determined that the model performed better for higher (15%) rather than lower (5%) percent open area (POA) samples. The slope error criteria indicated that the model's predictions were on average within 20% and 30% for the higher and lower (POA), respectively. The lower POA perforate numerical model predictions presented more scatter for different t/ds, in the slope and correlation error criteria, than at higher POA. The scatter also tended to increase as the flow velocity was increased for a given POA.

It is hypothesized that the model underpredicts the experiments because the measured raylometer $C_D$ is higher than the actual acoustic $C_D$ as indicated in Ref. 18. Also, at lower POAs the higher fluid velocities in the perforate's orifices start forming unsteady vortices, which is not accounted for in our model. Consequently the model performs better at the higher rather than lower POAs. The reader is referred to Ref. 19 if a higher bias flow velocity model is desired. Note Ref. 19 utilizes the $e^{-i\omega\tau}$ while this paper utilized the $e^{+i\omega\tau}$ convention.

The PBFIF model showed very good agreement with Premo's time domain model (Ref. 6) for all bias flow rates.

## Acknowledgements

A special thanks is issued to Tony Parrott and Mike Jones from NASA Langley Research Center for sponsoring this work. They have also reviewed this paper, and provided invaluable scientific insight and support.

## References

1. Dean, P. D., "On the In-Situ Control of Acoustic Liner Attenuation," ASME Paper No. 76-GT-61, Transactions of the ASME, *Journal of Engineering for Power.*
2. Kelly, J.J., Betts, J.F., Follet, J.I., and Thomas, R.H., "Bias Flow Liner Investigation," *Virginia Tech Report VPI-434487*, December 1999.
3. Hersh, A.S. and Rogers, T., "Fluid Mechanical Model of the Acoustic Impedance of Small Orifices," AIAA 75-495, March 1975.
4. Kelly, J.J. and Abu-Khajeel, H., "A User's Guide to the Zwikker-Kosten Transmission Line Code (ZKTL)," NASA/CR-97-206901, December 1997.
5. Premo, J., "The Application of a Time-Domain Model to Investigate the Impedance of Perforate Liners Including the Effects of Bias Flow," AIAA-99-1876. 1999.
6. Crandall, I.B., *Theory of Vibrating Systems and Sound,* D. Van Nostrand & Co. New York, 1927.
7. Melling, T.H., "The Acoustic Impedance of Perforates at Medium and High Sound Pressure Levels," *Journal of Sound and Vibration*, 29(2-1), 1973.
8. Sivian. L. J., "Acoustic Impedance of Small Orifices," *J. Acoustical Society of America*, Vol. 7, October 1935, pp. 94-101.
9. Tijdeman, H., "On the Propagation of Sound Waves in Cylindrical Tubes," *Journal of Sound and Vibration*, 39(1), 1975
10. Rschevkin, S.N. *A course of Lectures on the Theory of Sound,* Pergamon Press, London 1963.
11. Cataldi, P., Ahuja, K. K., and Gaeta Jr., R. J., "Enhanced Sound Absorption Through Negative Bias Flow," AIAA 99-1879, 1999.
12. Kraft, R.E., Yu J., and Kwan H.W., "Acoustic Treatment Design Scaling Methods," Volume 2, Advanced Treatment Impedance Models for High Frequency Ranges, NAS3-26617, May 1996.
13. James, M.L., Smith, G.M., and Wolford, J. C., *Applied Numerical Methods for Digital Computation*, Harper Collins College Publishers, 1993. pp. 302-305.

14. Bendat, J.S. and Piersol, A. G., *Random Data*, John Wiley & Sons, New York, 1986.
15. Jing, X. and Sun, X., "Numerical Simulation on the Nonlinear Acoustic Properties of an Orifice," AIAA-99-1878.
16. Jing, X. and Sun, X., "Effect of Plate Thickness on Impedance of Perforated Plates with Bias Flow," AIAA-99-1877.